Translational Oncology
www.transonc.com

Volume 10 Number 2 April 2017 pp. 229–240 229

Dual Functional Mesoporous Silicon Nanoparticles Enhance the Radiosensitivity of VPA in Glioblastoma[1]

Hailong Zhang*[2], Wei Zhang[†,2], Yong Zhou[†], Yuhua Jiang*[†] and Shupeng Li[*,†]

*Drug Innovation, The Second Hospital of Shandong University, Jinan, PR China; [†]Cancer Centre, The Second Hospital of Shandong University, 247 Beiyuan Street, Jinan, PR China

Abstract

Radiotherapy is a critical strategy and standard adjuvant approach to glioblastoma treatment. One of the major challenges facing radiotherapy is to minimize radiation damage to normal tissue without compromising therapeutic effects on cancer cells. Various agents and numerous approaches have been developed to improve the therapeutic index of radiotherapy. Among them, radiosensitizers have attracted much attention because they selectively increase susceptibility of cancer cells to radiation and thus enhance biological effectiveness of radiotherapy. However, clinical translation of radiosensitizers has been severely limited by their potential toxicity to normal tissue. Recent advances in nanomedicine offer an opportunity to overcome this hindrance. In this study, a dual functional mesoporous silica nanoparticle (MSN) formulation of the valproic acid (VPA) radiosensitizer was developed, which specifically recognized folic acid–overexpressing cancer cells and released VPA conditionally in acidic turmeric microenvironment. The efficacy of this targeted and pH-responsive VPA nanocarrier was evaluated as compared to VPA treatment approach in two cell lines: rat glioma cells C6 and human glioma U87. Compared to VPA treatment, targeted VPA-MSNs not only potentiated the toxic effects of radiation and led to a higher rate of cell death but also enhanced inhibition on clonogenic assay. More interestingly, these effects were further accentuated by VPA-MSNs at low pH values. Western blot analysis showed that the effects were mediated via enhanced apoptosis-inducing effects. Our results suggest that the adjunctive use of VPA-MSNs may enhance the effectiveness of radiotherapy in glioma treatment by lowering the radiation doses required to kill cancer cells and thereby minimize collateral damage to healthy adjacent tissue.

Translational Oncology (2017) 10, 229–240

Introduction

Glioblastoma is the most common type of primary malignant brain tumor in adults not only for its poor prognosis [1] but also its direct repercussions on quality of life and cognitive function [2]. Clinically, radiation therapy (RT) is the standard adjuvant approach for glioblastoma to suppress tumor proliferation through inducing DNA damage or free radical damage in tumor sites [3,4]. However, irradiative side effects caused by the poor discrimination between normal and tumor limit the further clinical implementation of radiotherapy [5].

Development of radiation sensitizers is required for radiotherapy to enhance the cancer-killing effects while minimizing cytotoxicity to surrounding tissues. Among various radiation sensitizers, histone deacetylase (HDAC) inhibitors sensitize cancer cells to ionizing radiation and induce growth arrest, differentiation, and apoptosis of

Address all correspondence to: Shupeng Li or Jiang Yuhua, Cancer Centre, The Second Hospital of Shandong University, 247 Beiyuan Street, Jinan, Shandong, 250033, PR China. E-mail: sdeylsp@gmail.com

[1] This work was supported by the National Natural Science Foundation of China (No. 81371470) and Shandong Provincial Natural Science Foundation of China (No. ZR2010HM080).

[2]Equal Contributions.

Received 21 October 2016; Revised 12 December 2016; Accepted 19 December 2016

1936-5233/17
http://dx.doi.org/10.1016/j.tranon.2016.12.011

cancer cells *in vitro* and *in vivo* [6–8]. Valproic acid (VPA), a commonly prescribed antiepileptic drug for the treatment and prevention of seizures in brain tumor patients [9], has been shown to be an effective inhibitor of HDAC [10,11]. VPA could acetylate core histone proteins H3 and H4, modulate chromatin structure and gene expression [12], and enhance the radiosensitivity of a variety of tumor cell types [13–15].

Although relatively safe, VPA causes various toxic and side effects on higher concentrations [16], including hepatotoxicity [17], neurotoxicity [18], and teratogenicity [19], which severely limits its clinical utility [20]. Aiming at minimizing radiation damage to normal tissue without compromising therapeutic effects on cancer cells, the development of targeted and controlled-release system for VPA delivery is an urgent need. During the past decades, mesoporous silica nanoparticles (MSNs) have been developed as a novel targeted and controlled-release system due to their selectivity and applicability in drug delivery. MSNs have stable physicochemical and biochemical profiles. They are inherently immune to hydrolysis and enzymatic degradation. Also, the extensive mesoporosity and pore volumes enable them to hold extraordinarily large loadings of drugs, thus significantly enhancing drug treatment efficacy while avoiding its side effects, making them a biocompatible load vehicle [21]. Taking advantage of the large surface areas of MSNs that allowed easy and efficient facile surface functionalization, efforts have been put to precisely control drug release in response to external and internal stimulus. Accordingly, a number of external control mechanisms have been tested, including magnetic fields, near-infrared light, and radiofrequency heating [22]. Several other internal stimuli are also employed to modulate the drug release profile, including extracellular/intracellular pH changes, redox potentials, enzyme-based cleavage, and also temperature changes [23].

In order to maximize therapeutic effects against cancer, numerous measures have focused on controlling drug release at the tumor microenvironment or inside cancer cells [22]. Among them, pH-responsive nanocarriers are particularly valuable for they can exploit the inherent pH gradients present in the tumor microenvironment and also in lysosomal trafficking pathways inside cancer cells to trigger the release of bioactive molecules [24]. In fact, the average extracellular tumor pH is slightly acidic (ranging from pH 5 to pH 7) due to increased lactate production in tumors, whereas in most tissues and blood, the extracellular pH is approximately 7.4 [25]. This difference opens an opportunity window to promote pH-responsive drug release in tumors. In this study, we have designed a dual-switch mesoporous silica–based therapeutic agent, which directly delivers VPA into the cancer cells for greatly enhanced damage of the DNA on irradiation, thus effectively enhancing the radiotherapy efficacy to kill tumor cells (Supplemental Figure 1).

Experimental Procedures

Methods

All chemicals and solvents were purchased from commercial sources and were used as received, unless otherwise noted. Valproic acid, β-cyclodextrin, MTT (3-[4,5-dimethylthiazol-2-yl]-2,5- diphenyltetrazolium bromide; thiazolyl blue), cetyltrimethyl ammonium bromide (CTAB), tetraethyl orthosilicate (TEOS), (3-aminopropyl)-triethoxysilane (APTES), 3-iodopropyltrimethoxysilane (IPTMS), benzimidazole, toluene (anhydrous), fluorescein, 2′,7′-dichlorofluorescein diacetate (DCFDA), Hoechst 33258, calcein blue, and propidium iodide (PI) were obtained from Sigma (St. Louis, MO). Dulbecco's modified Eagle's medium (DMEM), fetal bovine serum (FBS), penicillin, and streptomycin were obtained from Gibco BRL (Grand Island, NY). Antibodies for P53, caspase-3, and PARP were obtained from Cell Signaling Technology (Danvers, MA). Monoclonal antibodies for Bcl-2 (50E3) and PARP (46D11) were purchased from Santa Cruz Biotech (Santa Cruz, CA). Monoclonal antibody for Bax (ab5714) was from Abcam (Cambridge, UK). Bicinchoninic acid (BCA) protein assay kit and ECL chemiluminescence system were obtained from Pierce (Rockford, IL) and GE Healthcare (Piscataway, NJ), respectively. Annexin V–fluorescein isothiocyanate (FITC) Apoptosis Analysis Kit (AO2001-02P-H) was purchased from Sungene Biotech (Tianjin, China).

Preparation of Benzimidazole-Functionalized MSNs

MSNs were prepared according to our previous study [26]. A total of 480 ml of CTAB in 15 mM NaOH solution (2.1 mg/ml) was slowly heated up to 80°C in 30 minutes before dropwise addition of 5 ml of TEOS in 10 minutes. Vigorous stirring was conducted to avoid formation of giant particles. After addition, the white suspension was continually stirred for 2 hours at 80°C to attain uniform nanoparticles. Rude silica nanoparticles were obtained after centrifuge and washed for four times by deionized water and methanol, respectively. Finally, the CTAB surfactant from inside of nanoparticles was removed by refluxing for 24 hours in methanolic solution [160 ml of methanol and 9.00 ml of HCl (37.4%)] to gain MSNs. The formed MSNs were washed with deionized water and methanol extensively, followed by drying at 60°C over 48 hours, and kept at 4°C for long storage.

To prepare benzimidazole-functionalized MSNs, 100 mg of prepared MSNs was added into 100 ml of anhydrous ethanol with stirring. Then, 20 μl of IPTMS was added dropwise, and the solution was refluxed at N_2 atmosphere for 12 hours to attain MSN benzimidazole functionalization. Then, the reacted mixture was filtered to remove ethanol and unreacted IPTMS, followed by washing with deionized water and DMF for four times, respectively. Finally, benzimidazole-functionalized MSNs were achieved by drying in the vacuum over 72 hours to remove H_2O completely.

To yield amine/benzimidazole-functionalized MSNs, 100 mg of prepared benzimidazole MSNs and 50 μl of APTES were refluxed in 100 ml of dry toluene at nitrogen atmosphere for 24 hours. After removal of toluene, the resulting functional MSNs were then washed with ethanol and deionized water for four times, respectively. Finally, the product was dried at 70°C over 48 hours to remove H_2O completely and kept in 4°C for long storage.

To prepare folate/benzimidazole-functionalized MSNs, 10 mg of folate-PEG3400-COOH was dissolved in degassed 0.1 M 2-[morpholino]ethanesulfonic acid buffer (pH 7.4) containing 4 mg EDC and 1 mg NHS, and stirred for 30 minutes at RT to attain activated MSNs. The MSNs solution above was adjusted to pH 7.4 and mixed with 100 mg of folate/benzimidazole-PEG3400-MSNs for 24 hours. After complete washing by deionized water, folate/benzimidazole-functionalized MSNs were dried in the vacuum and kept in 4°C with N_2 atmosphere for long storage.

To prepare fluorescence labeled MSNs, 2.5 mg of FITC was stirred with 40 μl N-(2-aminoethyl)-3-aminopropyltrimethoxysilane in 1 ml of absolute ethanol in the dark for 2 hours at room temperature. A total of 40 mg folate/benzimidazole-functionalized MSNs was suspended in 1 ml of solution above and stirred at 60°C

for 10 hours in the dark. The FITC-labeled MSNs were centrifuged and washed with ethanol and H_2O. After drying in the vacuum, the product was covered by aluminum foil and kept in 4°C with N_2 atmosphere for long storage.

Characterization of MSNs

The morphology and mesostructure of MSNs were observed via scanning electron microscope (SEM, EX-250 system) and transmission electron microscopy (TEM, JEM-1200EX). TEM micrographs were obtained on a JEM-2010 electron microscope with an accelerating voltage of 200 kV and SEM at 10 kV. Fourier transform infrared spectroscopy (FTIR; Equinox 55 IR spectrometer) was used to characterize the structure information on MSNs.

Preparation of VPA Loaded MSNs

MSN-benzimidazole was dissolved in valproic acid sodium salt solution (50 mg/ml) to reach 100 μg/ml. The solution is sonicated for 3 × 5 seconds to dissolve the MSNs completely. The solution above was mixed at room temperature for 12 hours in rotation (reversely) or stirred by magnesium bar. Then, β-cyclodextrin was added to reach 50 mg/ml and mixed for another 12 hours. The nanoparticles were centrifuged and washed with tridistilled water three times for immediate using (if not, keep the solution in step 4 at 4°C); then, cell culture medium was added to reach 100 μg/ml of MSN nanoparticles.

Cell Culture and Treatment

Rat C6 glioma cell line (serial no. 3111C0001CCC000131) was obtained from the Cell Resource Centre (Chinese Academy of Medical Sciences, Beijing, China), and human U87 glioma cell line was a gift from Dr. Ye L (Cancer Center, The Second Hospital of Shandong University, Jinan). Cells were cultured in DMEM (and 10% fetal bovine serum; both from HyClone, Logan, UT) at 37°C under a humidified atmosphere containing 5% carbon dioxide and maintained in an exponential growth state. The adherent cells were collected by using 0.25% trypsin. VPA was added prior to irradiation (3 Gy/min, 6 MV, X-ray), which was performed in warm culture medium. The cells were irradiated using an Elekta Synergy (Stockholm, Sweden) X-ray source. Dosimetry was performed by ion chamber and chemical Fricke dosimetry.

Fluorescence Confocal Microscopy Measurements

To study the cell targeting and endocytosis of MSN materials, fluorescence confocal microscopy was employed. Polylysine-coated coverslips were placed in six-well plates. C6 or HEK293 cells were seeded and grown for 30 hours on the coverslips. After 30 hours, the cells were incubated with 10 μg/ml of MSNs and grown for an additional 12 hours. Then, the growth medium was removed, and the cells were washed with PBS and incubated with Hoechst 33258 for 15 minutes to stain the cell nucleus. Coverslips were fixed to glass slides with adhesive. Images were taken and merged under green channel from FITC (488/520 ± 10 nm), blue channel from Hoechst 33258 (340/461 nm ± 10 nm), and red channel from doxorubicin (470/585 ± 10 nm). Red fluorescence generated by doxorubicin was loaded into MSNs as a replacement of VPA to observe the cargo release.

MTT Assay

MTT assay was performed as instructed by the manufacturer to assess cell viability. Briefly, C6 and U87 glioma cells were seeded in two 96-well plates (approximately 5000 cells/well). VPA, MSNs, and VPA-MSNs were diluted to different concentrations (12.5, 25, 50, and 100 mg/ml) and added into the cells. After specific time periods (24 and 48 hours) of incubation, 20 μl of MTT (5 mg/ml) was added to each well for 4 hours. Then, 150 ml of DMSO (Sigma, D2650) was added to each well and agitated for 10 minutes at room temperature. Optical density (OD) was measured at 570 nm on a Bio-Rad microplate reader (Hercules, CA). The value of experimental OD value/control OD was the proliferation index value. Data points were calculated from three independent experiments.

Flow Cytometry Analysis

The specified numbers (1×10^6/ml) of C6 and U87 glioma cells in single cell suspensions were seeded in individual wells of 6-well plates and incubated for 24 h at 37°C prior to treatment with VPA, MSNs, and VPA-MSNs at indicated concentrations (25 mg/l, 100 mg/l, pH 6 100 mg/l, adjusting culture medium pH to 6 for 30 minutes) for 6 hours or with PBS as a control, followed by irradiation (0, 4.0, and 8.0 Gy). After incubation for an additional 24 hours, the harvested cells were digested, collected, and centrifuged at a speed of 1500 rpm for 10 minutes. Apoptosis was detected in cells washed with PBS by staining with Annexin V–FITC and PI for 15 minutes at 4°C in the dark. Stained cells were analyzed by Becton-Dickinson (Franklin Lakes, NJ) flow cytometer and ModFit LT software (Verity Software House, Topsham, ME). Values were expressed as the mean ± standard deviation (SD).

Clonogenic Assay and Estimation of Sensitizer Enhancement Ratio (SER)

To evaluate radiosensitivity, cells were divided into four groups according to treatments of nanoparticles and VPA: the irradiation group, the VPA (10 mg/l, 100 mg/l) + irradiation group, the MSNs (10 mg/l, 100 mg/l, pH 6 100 mg/l) + irradiation group, the VPA-MSNs (10 mg/l, 100 mg/l, pH 6 100 mg/l) + irradiation group. These groups were further divided into five subgroups according to the radiation doses: 0-, 2.0-, 4.0-, 6.0-, or 8.0-Gy irradiation. Viable tumor cells per dose and substance were counted and plated into each culture dish in drug-free culture medium containing 10% fetal calf serum. After 10 to 14 days, the numbers of colonies (more than 50 cells) were counted, which were normalized to those observed in the unirradiated controls. The SER was calculated as the radiation dose needed for radiation alone divided by the dose needed for various concentrations of the VPA, MSNs, or VPA-MSNs nanoparticles.

Western Blot Analysis

Expressions of caspase-3, PARP, Bax, and Bcl-2 were determined by immunoblot analysis after treatment of VPA, MSNs, VPA-MSNs, and pH 6 VPA-MSN and radiation in C6 cells and U87 cells. The cells were lysed in RIPA buffer containing phenylmethanesulfonyl fluoride after washing with cold PBS twice, and then samples were centrifuged at 12,000 ×*g* for 20 minutes at 4°C. The proteins were quantified using BCA assay and separated by 6% to 15% SDS-PAGE and transferred onto nitrocellulose membranes according to the manufacturer's instructions. Membranes were blocked with 5% nonfat milk at 37°C for 2 hours and then incubated with rabbit polyclonal anti–caspase-3, anti-PARP, anti-Bax, anti-Bcl, or mouse anti–β-actin antibody at 1:2000 dilution overnight at 4°C. The membranes were then washed three times in TBS-T, incubated with the appropriate FITC-conjugated secondary antibodies at a 1:5000

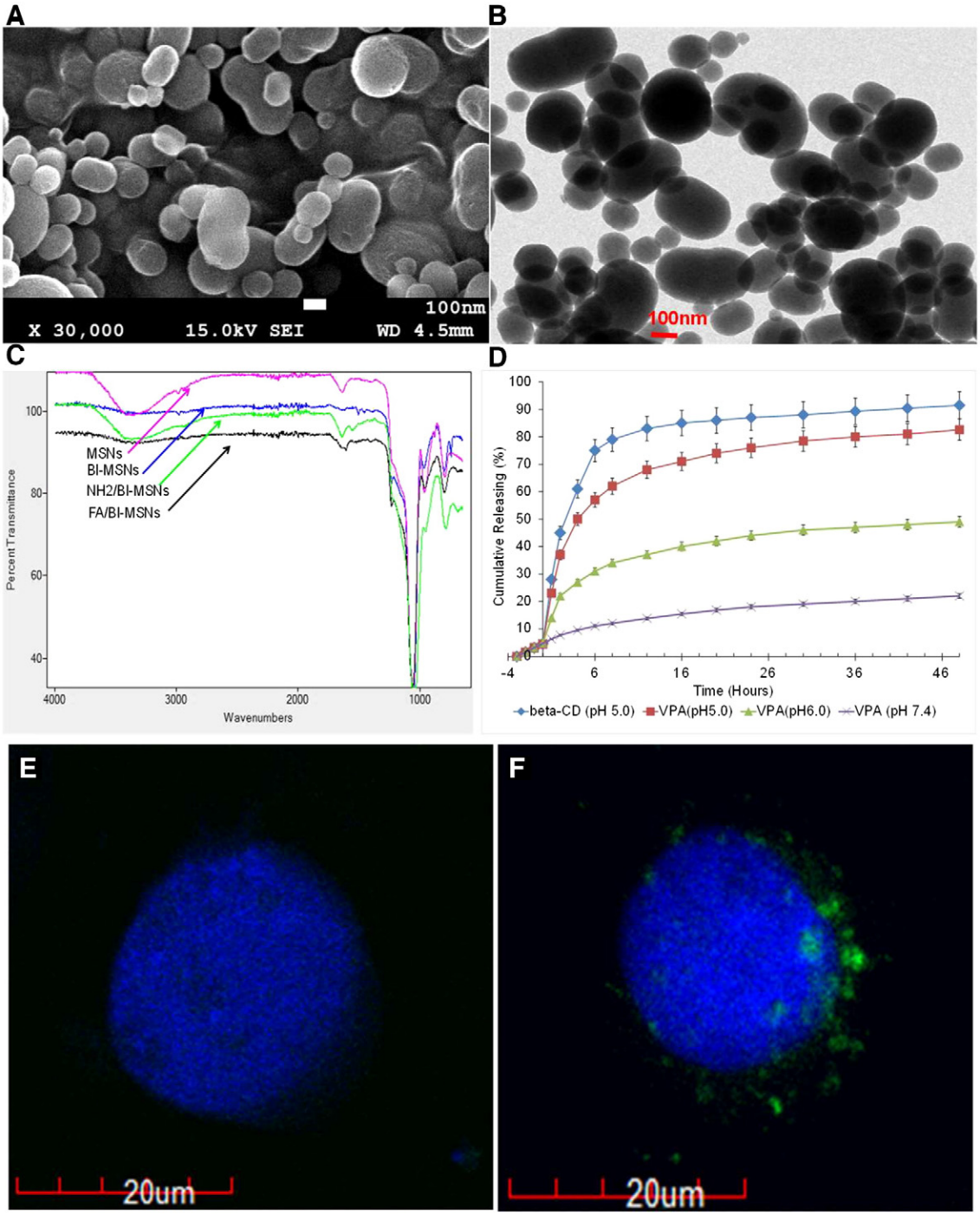

Figure 1. Characterization of MSNs and VPA releasing profiling. (A) SEM image of MSNs. (B) TEM image of MSNs. (C) FTIR spectra of MSNs: nonfunctionalized (control), benzimidazole functionalized (BI-MSNs), amine functionalized (NH2/BI-MSNs), and folate grafted MSNs (FA/BI-MSNs). (D) Releasing profiling of beta-CD and VPA from FA/BI-MSNs in different condition. Release of VPA salt was monitored using HPLC-MS with positive mode. (E and F) Confocal microscopy images of HEK-293 (FR−, E) and C6 (FR+, F) cells after treatment with 10 μg/ml of MSN@FITC for 12 hours. Images are taken and merged under green channel from FITC (488/520 ± 10 nm) and blue channel from Hoechst 33258 (340/461 nm ± 10 nm). For HEK-293 cells where FR is not expressed, minimal unspecific binding of MSN@FITC could be found (E). For C6 cells expressing FRs, massive folic-MSN@FITC binding was observed (F).

dilution in blocking solution for 1 hour at room temperature, and subsequently washed thoroughly three times in TBS-T. β-Actin was used as a loading control. Proteins were visualized by enhanced chemiluminescence (Millipore). Images were processed with Image J software (NIH, USA) for densitometric quantification.

Statistical Analysis

Results were expressed as mean ± SE of at least three independent experiments and analyzed with one-way analysis of variance (ANOVA) tests. For clonogenic assay, two-way ANOVA analysis was employed. Where significant difference was detected, the post

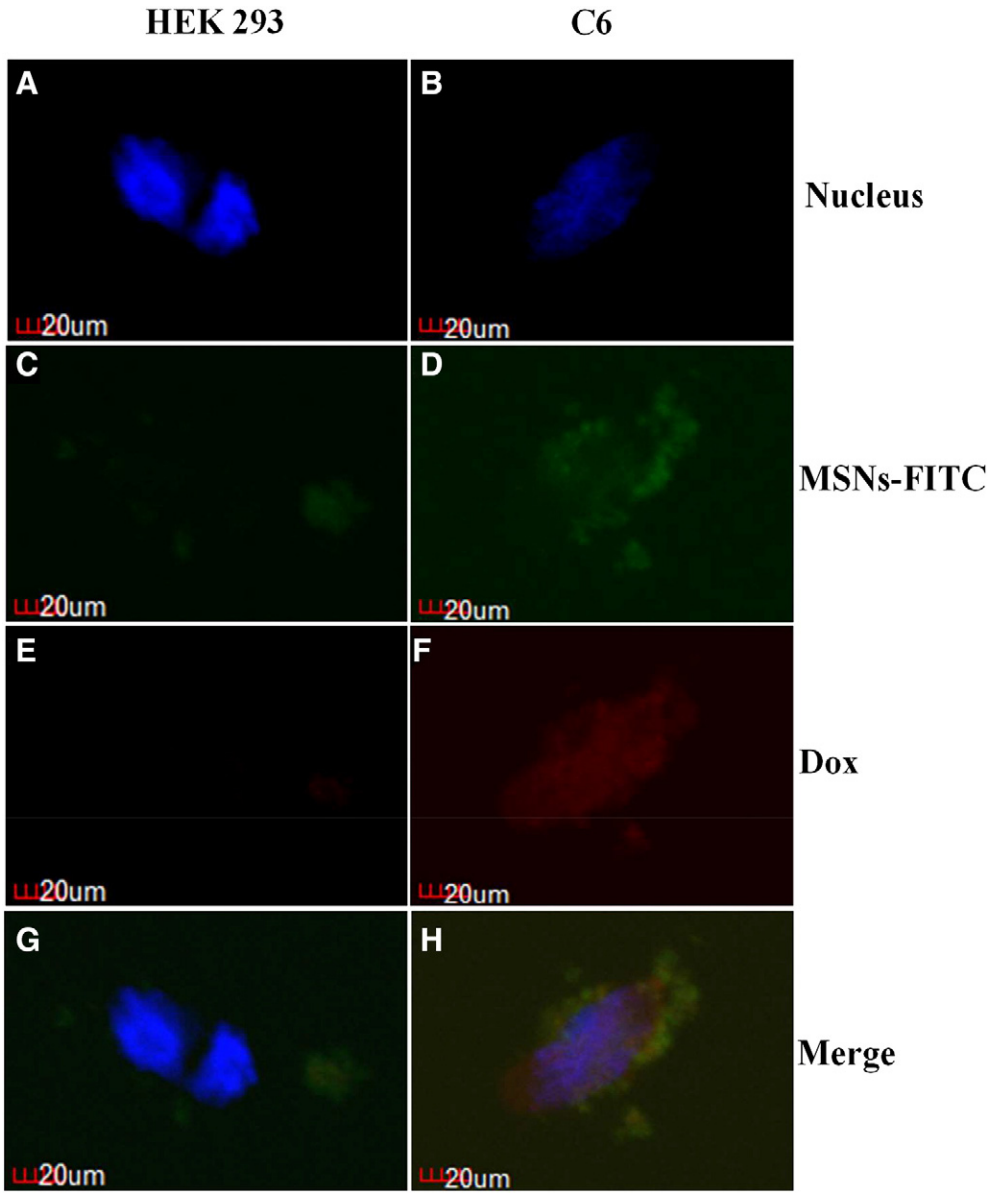

Figure 2. Dual-function MSN showed specific binding and intracellular releasing. Confocal microscopy images of HEK-293 (FR−, A, C, E, G) and C6 (FR+, B, D, F, H) cells treated with doxorubicin-MSN@FITC (C to F) for 12 hours. Images are taken and merged under green channel from FITC (488/520 ± 10 nm), blue channel from Hoechst 33258 (340/461 nm ± 10 nm), and red channel from doxorubicin (470/585 ± 10 nm). For HEK-293 cells where FRs were not expressed, minimal unspecific binding of MSN@FITC could be found. For C6 cells expressing FRs, massive folic-MSN@FITC binding (B, D, F, H) and intracellular releasing of doxorubucin could be observed (F).

Newman-Keuls test or Bonferroni test was applied. Data analysis and statistical comparisons were performed using Graphpad PRISM program (Graphpad Software, La Jolla, CA). A value of $P < .05$ was considered significant.

Results and Discussion

Design, Preparation, and Characterization of Folate/Benzimidazole-Functionalized MSNs

In this study, a sub–150- to 200-nm tumor cell targeting dual-switch MSNs system was designed to directly deliver VPA into cancer cells for enhanced damaging of the DNA with irradiation. The synthesized pH-responsive targeted delivery system could selectively deliver and control releasing VPA into tumor cells, which is expected to achieve substantially enhanced synergetic chemo-/radiotherapy under the monitoring of MR/UCL bimodal imaging.

To specifically target glioblastoma cells, MSNs surface modified by folate ligand that selectively binds folate receptors expressed in glioblastoma cells was synthesized. To control VPA release in tumor, a well-established pH-responsive host-guest system of the aromatic amino group (benzimidazole) and β-cyclodextrin has been exploited to prevent VPA leaking out from the pore and releasing in acid environment (pH < 6.0). The radiation sensitizer VPA as a payload was employed to enhance the effectiveness of radiation in the treatment of GMB cells. As illustrated in Supplemental Figure 2, folate/benzimidazole functionalization of MSNs has been accomplished by

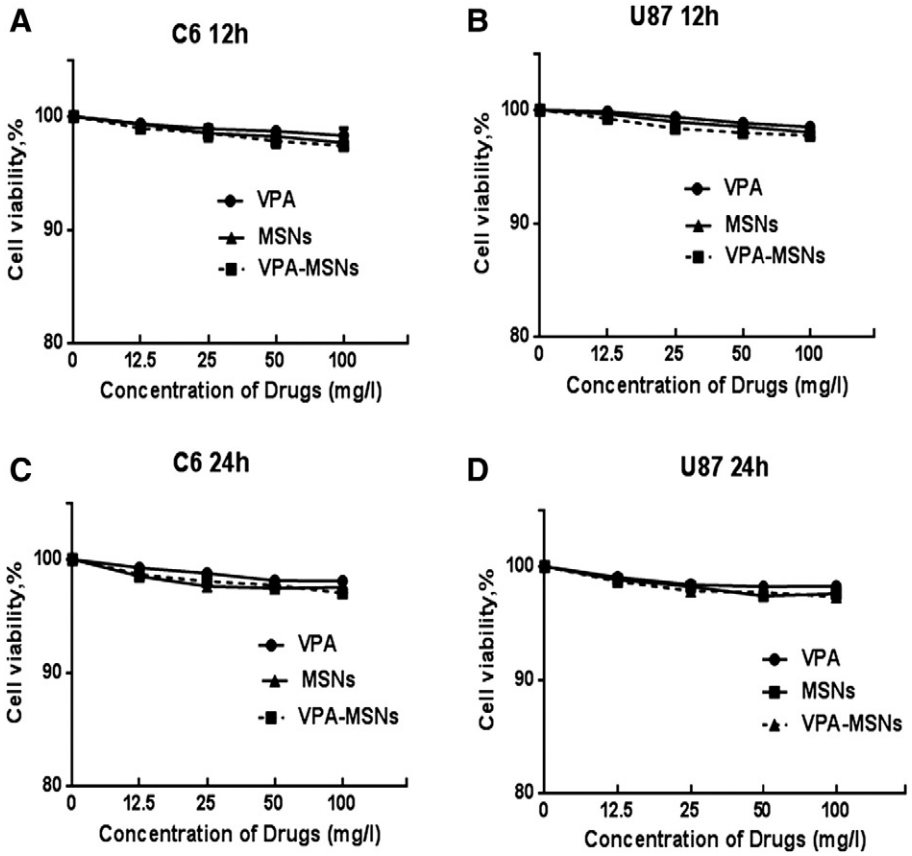

Figure 3. Effect of VPA, MSNs, and VPA-MSNs on C6 and U87 glioma cell viability. C6 and U87 gliomas were treated with various concentrations of VPA, MSNs, and VPA-MSNs for 12 or 24 hours, and cell viability were examined with MTT assay. Cell viability was calculated relative to untreated controls.

two steps: benzimidazole introduction and folate attachment of MSNs. MSNs were first prepared and then functionalized with 3-iodopropyltrimethoxysilane to couple with a benzimidazole molecule through a nucleophilic substitution reaction. Next, APTES reacted with hydroxyl groups of MSNs to make surface amine functionalization. The introduced amine groups of MSNs further reacted with NHS ester–functionalized and PEGylated folate to yield folate/benzimidazole-functionalized MSNs. SEM and TEM micrographs revealed that synthesized MSNs have a cylindrical mesoporous structure with an elongated rod shape (Figure 1, *A* and *B*). Its size distribution was confirmed by TEM with the length and width of 180 and 120 nm, respectively. The successful introduction of benzimidazole group and later folate grafting to MSNs surface were confirmed by FTIR (Figure 1*C*). The absorption band of Si-O-Si at 1080 cm^{-1} was observed. The strong absorption band around 1400 to 1650 cm^{-1} for –C = N– stretching and 2800 to 3300 cm^{-1} for C–H and –NH stretching suggested successful incorporation of benzimidazole group. The formed covalent amide bond at 1620 cm^{-1} (covalent amide bond), 1563 cm^{-1} (–NH bond), and 1485 cm^{-1} (phenyl ring of folic acid) further confirmed the conjugation of folic acid to MSN surface via ECD/NHS coupling strategy. Further, the decreased absorption at 3400 cm^{-1} also indicated successful functionalization via amide bond formation. These features enabled MSNs to target specific tissue and intranuclear of the cells and responsively release payloads in the targeted sites in a sustained-release way.

Table 1. IC50 Values of the VPA and MSNs

IC50 (M ± SD)	VPA (mg/l)	MSNs (mg/l)	VPA-MSN (mg/l)
C6 12 h	77,387 ± 11,624	37,550 ± 15,500	58,456 ± 18,205
U87 12 h	55,415 ± 24,484	28,279 ± 11,175	52,923 ± 22,632
C6 24 h	51,731 ± 10,796	71,729 ± 12,546	54,067 ± 24,829
U87 24 h	80,096 ± 3654	76,343 ± 10,539	46,757 ± 6148

In Vivo Cargo Releasing Assay

As a stimuli-responsive nanocarrier, it is vital to release encapsulated cargos at targeted sites in an efficient and responsive way. We then examined VPA releasing profiling from both nonfunctionalized and folate/bifunctionalized MSNs. Mass spectrophotometer analysis was performed to measure VPA concentrations at *m*/*z* 310.2120 after dilution in MS running solution (50% acetonitrile with 0.1% formic acid). As shown in Figure 1, *C* and *D*, VPA molecules were effectively entrapped in the pore of folate/bifunctionalized MSNs, which exhibited good pore-capping property and precisely modulated release, reaching 76% release in 15 hours. In contrast, nonfunctionalized MSNs held much less VPA and slowly released it for more than 2 days, showing an unmodulated profile.

Targeted Delivery and Controlled-Release In Vitro Cells

In order to study the selective cell targeting efficiency of our MSNs system, two cell lines, HEK 293 and C6, with/without folic acid receptor (FR) expression, were employed (Figure 1, *E* and *F*). Selective cellular uptake of fluorescence (FITC)-labeled MSNs was

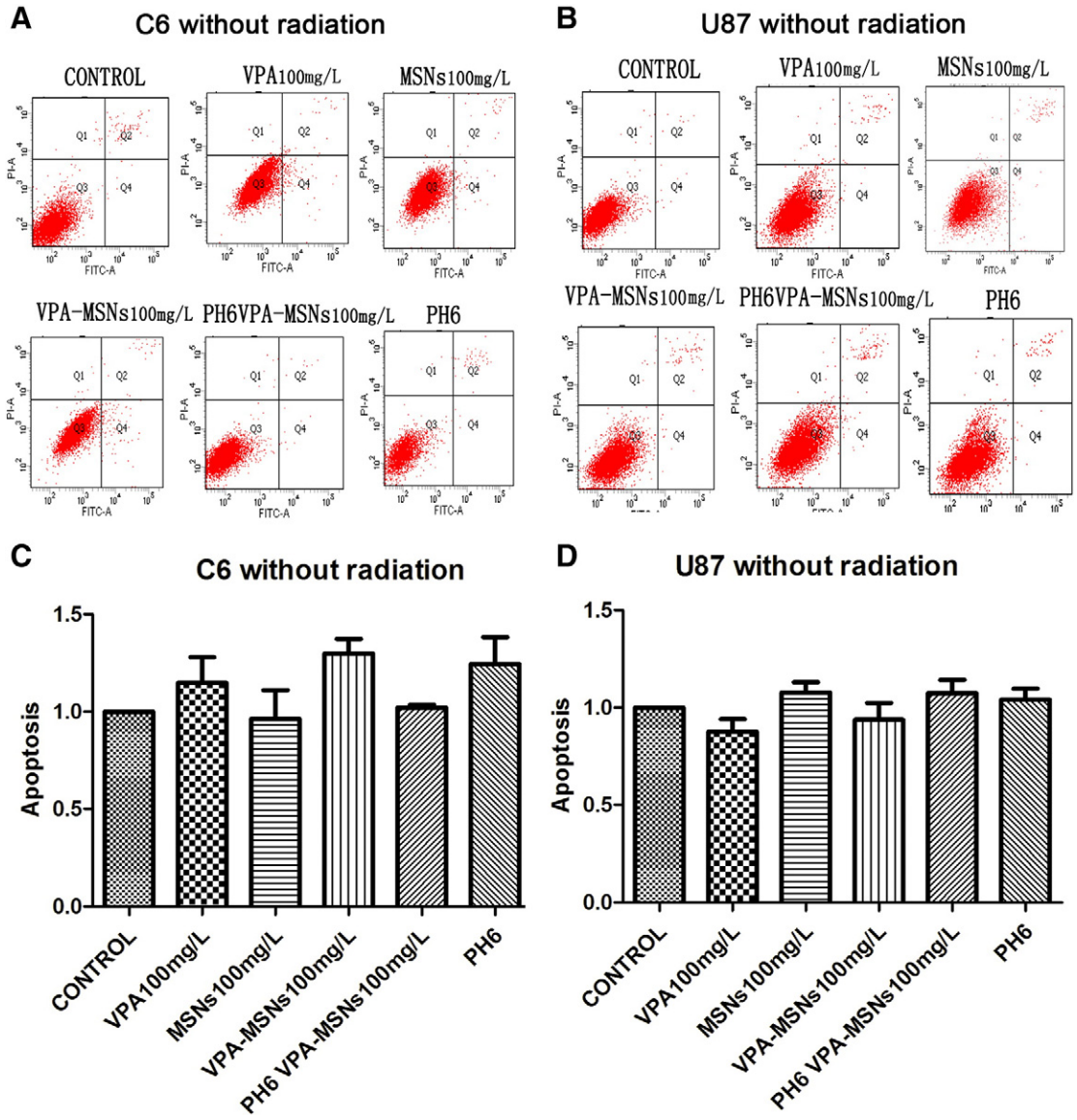

Figure 4. Flow cytometry of C6 and U87 cell apoptosis without irradiation. Flow cytometric analysis of cell apoptotic levels by PI and FITC–Annexin V fluorescence (A and B). The calculated apoptotic rates were shown in histograms (C and D). Without irradiation, no significant apoptosis was observed under VPA and MSNs treatment in both C6 and U87 cells. No distinguishable changes of apoptotic rate can be acquired from the calculation. There was also no significant apoptosis under VPA-MSNs treatment in pH 6.0 compared with VPA-MSNs treatment or the control in PBS (pH 7.4).

examined with confocal microscopy. HEK 293 cells incubated with folic-functionalized MSMs loaded with fluorescein only showed background fluorescence (Figure 1*E*), indicating low nonspecific binding of functionalized MSNs in FR-negative cells. However, when C6 cells were incubated with folic acid–functionalized MSNs, significant fluorescence accumulation could be found as shown in Figure 1*F*. Taken together, these results clearly demonstrated VPA intracellular delivery with folic acid–functionalized MSNs through FR-mediated endocytosis with negligible nonspecific binding.

Next, the dual-functionalized MSNs enabled selective targeting, and efficient intracellular releasing in FR-expressing neuronal cells was studied using HEK-293 or C6 neuroblastoma cell line. Doxorubicin was loaded to evaluate intracellular release after uptake of MSNs (Figure 2). Confocal fluorescence microscopy images showed stronger green fluorescence intensity in C6 cells. Moreover, after incubation with C6 cells, MSNs was uptaken via FR-mediated endocytosis, and doxorubicin was responsively released under low-pH environment (Figure 2, *B*, *D*, *F*, and *H*). As a contrast, only low nonspecific binding could be observed in HEK 293 cells with minimal release of doxorubicin. Taken together, these results showed highly specific binding and pH-responsive intracellular releasing of dual-functionalized MSNs in FR-positive cells.

Effect of VPA, MSNs, and VPA-MSNs on C6 and U87 Glioma Cell Viability

To examine the effects of MSNs and VPA-MSNs on cell viability, C6 and U87 cells were treated with serial dilutions of VPA, MSNs, and VPA-MSNs (12.5, 25, 50, and 100 mg/ml) for 12 and

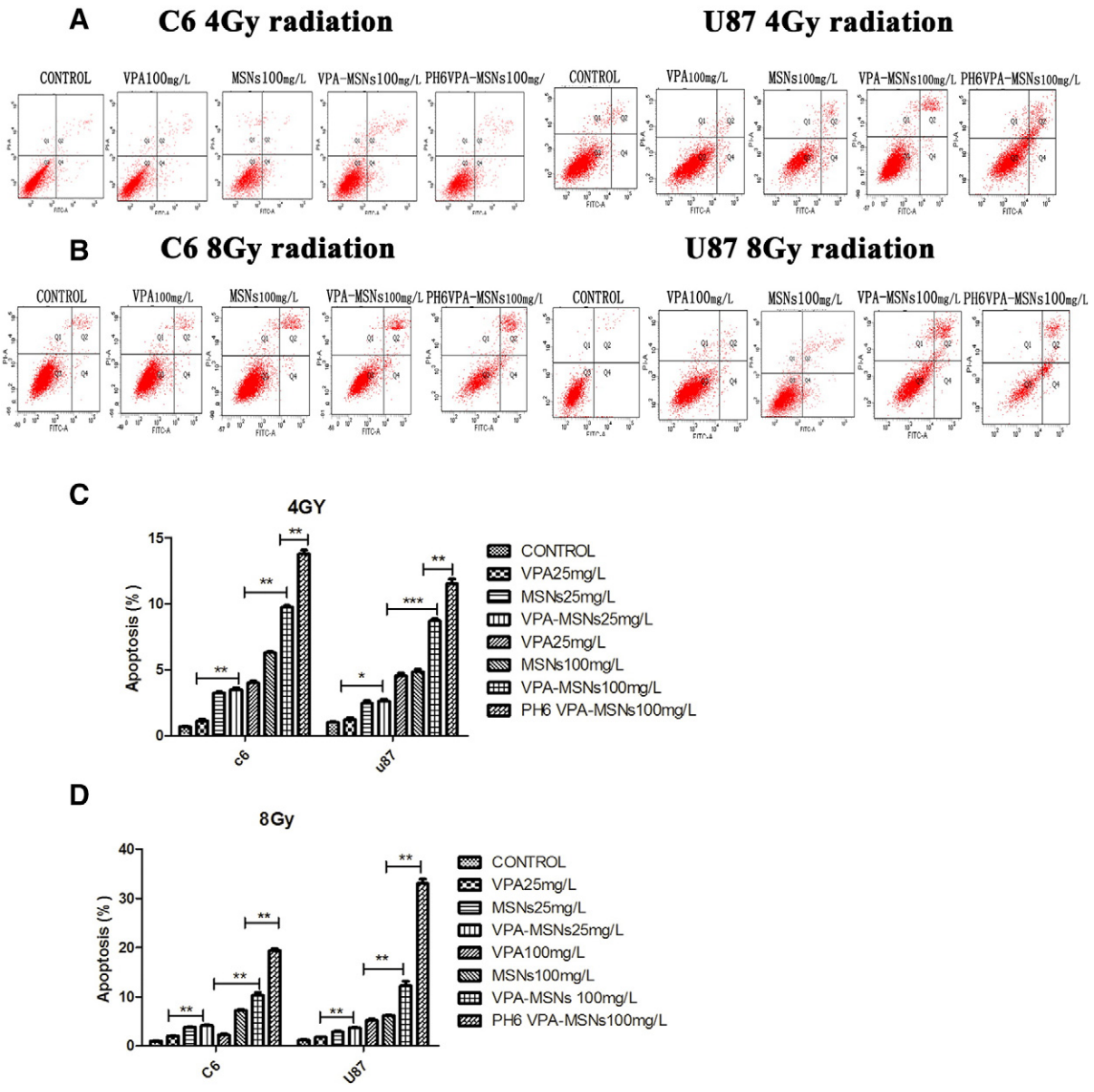

Figure 5. Flow cytometry of C6 and U87 cell apoptosis with 4- and 8-Gy radiation. (A) Cells were exposed to 4-Gy irradiation. A total of 100 μg/ml of nanoparticles caused increases in the apoptosis compared to the VPA group. A total of 100 μg/ml of nanoparticles treatment increased the apoptotic rate of C6, and in pH 6 conditions, the apoptotic rate was higher than in normal PH conditions. (B) Apoptotic rate was further increased with exposure to 8-Gy irradiation. (C and D). Histograms show changes of the apoptotic rate. With 4- and 8-Gy radiation, significant changes were observed in PH6 VPA-MSNs group compared with the VPA group or the control (*P < .05, **P < .01).

24 hours, respectively. As shown in Figure 3 and Table 1, MSNs and VPA-MSNs in either 10- or 100-mg/l concentrations did not induce remarkable cytotoxicity on C6 and U87 glioma cells.

Cell Apoptosis Analysis of C6 and U87 by Flow Cytometry

To investigate the effect of VPA-entrapped MSNs system on the therapeutic index of radiotherapy, flow cytometry assay was performed for qualitative and quantitative determination of cellular apoptosis under X-ray irradiation. As shown in Figure 4, without irradiation, no obvious apoptotic-inducing effects of VPA and MSNs on C6 and U87 cells could be observed. Both cells showed no significant difference of cellular apoptosis compared to the control groups on up to 100-μg/ml VPA-MSNs treatment (C6 cell: 1.06 ± 0.06% vs 0.98 ± 0.20%, P = .13; U87 cell: 1.03 ± 0.13% vs 0.94 ± 0.05%, P = .1). These results showed that VPA or MSNs had no significant cytotoxic effects on both C6 and U87 glioma cells. However, when cells treated with 100 μg/ml of VPA-MSNs were exposed to 4-Gy irradiation, significant increases in apoptosis could be observed compared to VPA group (9.75 ± 0.26% vs 0.68 ± 0.06%, P = .017) (8.71 ± 0.27% vs 1.01 ± 0.10%, P = .017) (Figure 5). The apoptotic rate was increased when exposed to high irradiation (8 Gy). Additionally, the apoptotic rate of C6 (13.76 ±

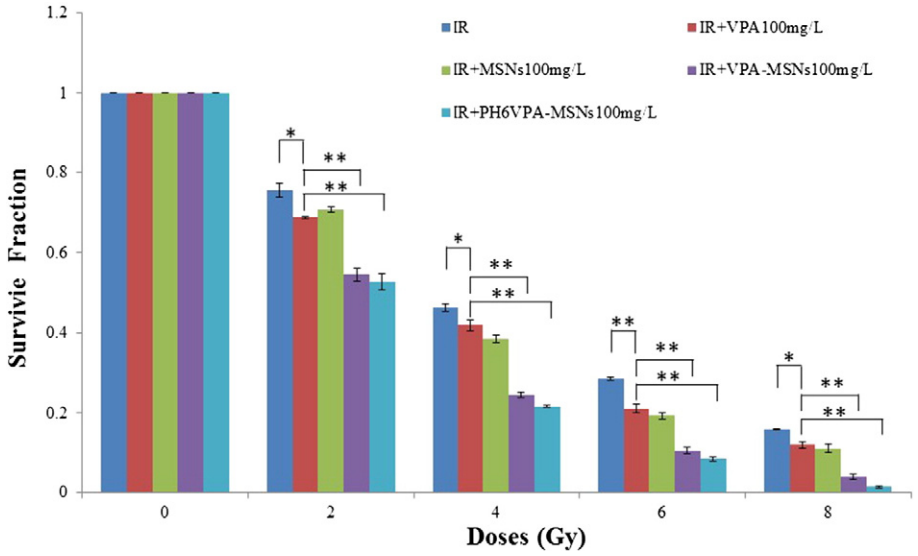

Figure 6. The colony formation assay of C6 cells. The IR-induced clonogenic survival was significantly reduced under VPA-MSNs treatment compared to cells treated with MSNs or VPA alone. Furthermore, the remarkable decrease in the number of cells was observed under acid condition (pH 6.0) (*$P < .05$, **$P < .01$).

0.52%) and U87 cell (11.54 ± 0.58%) under 100-μg/ml VPA-MSNs treatment was further enhanced in acid condition (pH 6.0). Together, pretreatment with VPA-entrapped MSNs dramatically enhanced C6 and U87 cellular apoptosis when exposed to X-ray irradiation as compared to VPA-only treatment. Acid condition further improved therapeutic index of radiotherapy due to pH-responsive MSNs system. As a control, the empty MSNs or VPA itself did not show obvious cytotoxicity without irradiation. Folic acid–functionalized and pH-responsive dual-functional MSNs system developed here could efficiently deliver VPA into intracellular cells (C6 and U87) via folic acid receptors and enhanced cytotoxicity effects caused by X-ray irradiation.

Effect of MSNs on VPA-Induced Radiosensitivity in C6 and U87 Glioma Cells

Furthermore, the augmented apoptotic responses in C6 and U87 cell (Figure 6) were used to account for the radiosensitization measured by clonogenic assay. To examine effects of VPA-MSNs on VPA-induced cell irradiation (IR) sensitivity, the clonogenic assay was performed. Log-phase cells were trypsinized and plated as single cells. After 6 hours of incubation to allow for cell attachment, cells were pretreated with 100 μg/ml of VPA, MSNs, VPA-MSNs, pH 6 VPA-MSNs for 16 hours and then exposed to 0-, 2.0-, 4.0-, 6.0-, and 8.0-Gy doses of IR. Colony survival was determined 14 to 20 days later. As shown in Figure 7, *A* and *B*, VPA-MSNs treatment remarkably potentiated the decreasing effects of 8-Gy IR on C6 cell numbers as compared to cells treated with VPA- or MSNs-only groups. A significant reduction in clonogenic survival with the addition of VPA-MSNs at pH 6 could be observed (Figure 7*B*). The SER for combined X-ray and VPA-MSNs at pH 6 compared to X-ray only was 1.7137. To further characterize the effects of the MSNs, the cell survival fraction was simulated by a multitarget click mathematical model. The SER in VPA-MSNs group was 1.506662, higher than the VPA group in C6 cells. In pH 6.0 conditions, the SER was 1.7137 higher than that in normal conditions (Table 2), respectively.

Western Blotting Analyses for Apoptotic Protein Expression

X-ray ionizing radiation causes DNA damage and subsequently induces apoptotic cell death, which is usually associated with caspase-dependent apoptotic pathway. A few key target proteins related to cell death including caspase-3, P53, Bax, Bcl-2, and poly-ADP-ribose polymerase (PARP) were studied by Western blotting to examine the radiotherapy efficacy to kill tumor cells under VPA-MSNs and X-ray irradiation. Cellular-delivered and pH-responsive releasing VPA by MSNs can inhibit HDAC, thus overriding the DNA damage defense response and facilitating the radiation-induced mitotic cell death via activation of the apoptotic signaling cascade. Representative Western blot and quantitative results of respective blot were shown in Figure 8. Three key proteins, activated caspase-3, P53, and PARP cleaved subunit, were significantly upregulated and Bcl-2 was downregulated when both cells were exposed to VPA-MSNs and VPA, all of which, in turn, promote further apoptosis and cell death. When treated by VPA or MSNs only, both cells did not show obvious enhancement in protein expression level (activated caspase-3, P53, Bax, and PARP cleaved subunit). Not surprisingly, treatment with VPA-MSNs and exposure to X-ray under acid condition (pH 6.0) further increased those protein expressions. The result showed that pretreatment with VPA-MSNs could enhance expression of caspase-3, P53, Bax, and PARP cleaved subunit and decrease Bcl-2 expression, and thus lead to activation of apoptotic signaling under X-ray exposure and enhance irradiation therapy efficacy.

Conclusions

Preclinical studies show that combinations of VPA and radiation inhibit double-stranded DNA repair and enhance malignant glioma's response to radiation especially for CNS tumors [27,28]. Investigators have noted that VPA increased radiosensitivity of glioma cell lines U251 and SF539. The synergistic tumor-growth delay effects could also be observed in animals treated with VPA and RT27. A number of clinical trials are pursuing such combination strategies such as VPA with temozolomide and radiation therapy in adult brain tumors.

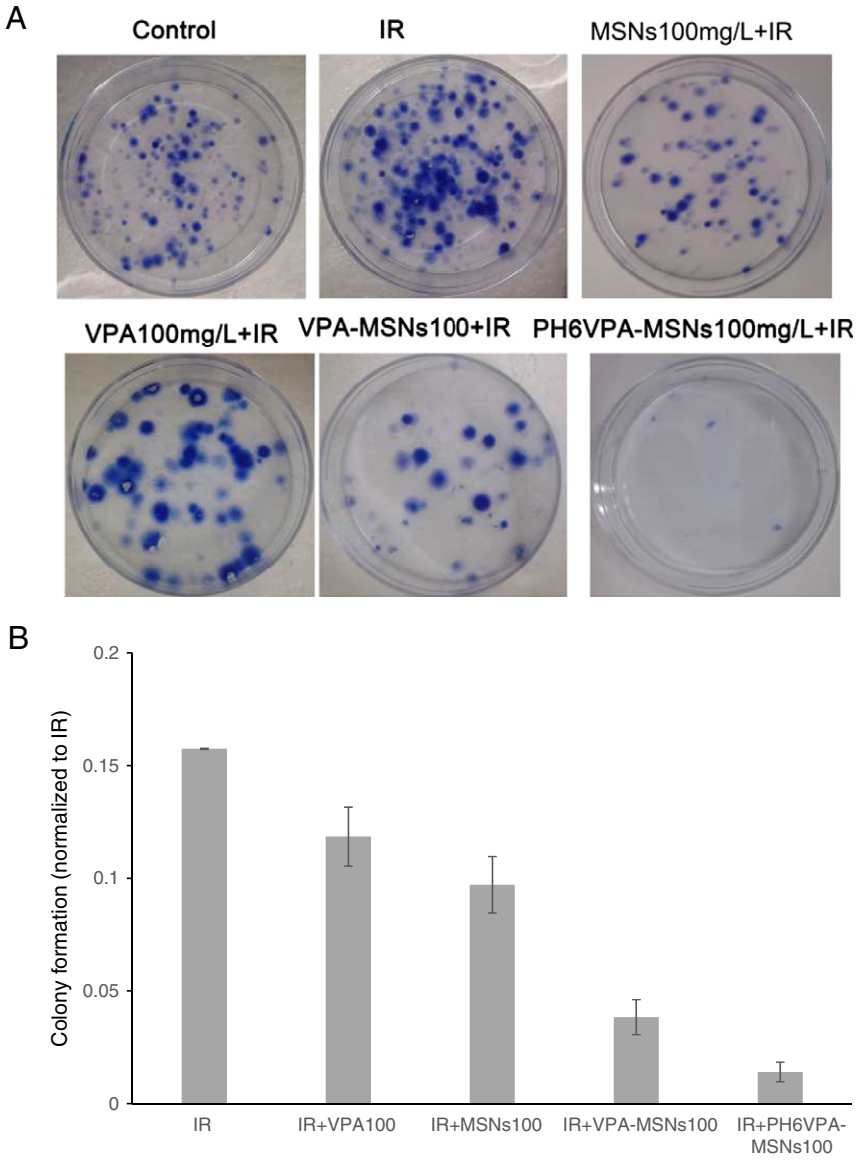

Figure 7. Clonogenic survival after VPA, nanoparticles, and IR exposure. (A) Clonogenic assay of C6 cells treated with VPA/or MSNs combined with 8-Gy IR; photographs of Petri dishes in a representative experiment are shown. (B) Percentage inhibition of colony formation as shown in A. Values represent the mean from three independent experiments. Error bars indicate 1 SD.

However, the combination is limited to VPA under the concentration of 100 mg/ml because of neurologic symptoms and other toxicities that arise [29,30]. Nanotechnology is considered as an effective strategy for cancer therapy owing to its customizable and multifunctional applications in tumor-targeted treatment [31–33] and selective drug delivery in tumor sites [34,35]. As an important carrier for targeted cancer therapy technology, nanodrugs play a vital role in solving the low selectivity of the drugs on the organs of tumor; they can reduce the adverse effects of drugs on nontarget site and improve drug efficacy but not reduce the effect [36]. The main purpose of our study is to look for particles which can enhance radiation efficacy, study the possible mechanisms of radiation-enhancing effects after entering the tumor cells, and reveal the potential impact of nanoscale radiation biology.

Table 2. Coefficients SER and Do Calculated for C6 Cells Irradiated by IR

Treatments	10 mg/l of VPA	10 mg/l of MSNs	10 mg/l of VPA-MSNs	10 mg/l of VPA-MSNs at pH 6	100 mg/l of VPA	100 mg/l of MSNs	100 mg/l of VPA-MSNs	100 mg/l of VPA-MSNs at pH 6
SER	1.047807	1.114035	1.203947	1.084649	1.09122	1.196789	1.506662	1.7137
Do	4.185852	3.937008	3.642987	4.043672	3.13087	2.854696	2.267574	1.99362

Do is calculated according to the curve and represents the average lethal dosage of cells, which indicates the repair ability of cells to sublethal injury. Subsequently, the SER may be calculated by the following equation: SER = Do value of X-ray group/Do value of combined group.

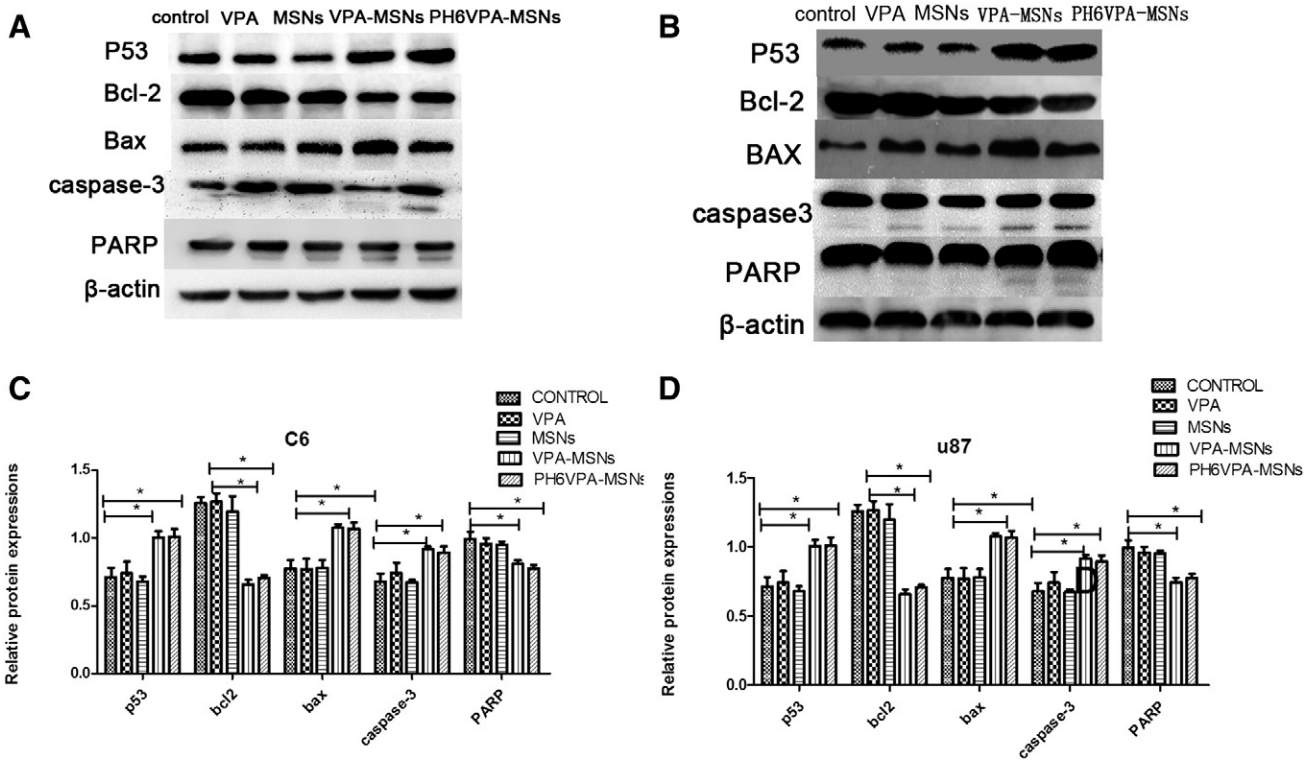

Figure 8. Western blotting analysis for P53, Bax, Bcl-2, caspase-3, and PARP. Different expression of apoptotic biomarkers (P53, Bax, Bcl-2, caspase-3, and PARP) under treatment with VPA-MSNs, VPA, and/or MSNs when exposed to X-ray (A and B). Quantitative expression changes of proteins P53, Bax, caspase 3, and Bcl-2 are shown in histograms (C and D) (*$P < .05$, **$P < .01$).

In our study, we choose VPA-MSNs as a starting point to explore its impact on radiation therapy.

Folate is a low-MW vitamin and plays an important role in 1 carbon transfer unit required for nucleotide production. We chose folic acid as the functional ligand due to its high stability, low immunogenicity, unlimited availability, compatibility with both organic and aqueous solvent, ability to conjugate with a great many molecules, and limited effects on the dimensions of the carrier [37]. Moreover, the receptor for folic acid (FR) is a cell-proliferation protein that is overexpressed in many types of cancer cells, including breast, kidney, head and neck [38,39], lung, colorectal [40], uterus, and ovary cancer [41,42]. Meanwhile, FR has a low expression on the apical surface of most normal cells5. This difference in expression makes FR a very attractive therapeutic target for novel tumor-specific agents.

The acid-elicited release is a novel profile found for NPS. Due to the poor delivery of oxygen and elevated glycolytic activity, H+ production and excretion are generally increased in cancers [43,44]. Furthermore, most tumors develop an aberrant vasculature network that hampers the ability of the microenvironment to remove tumor derived acid through diffusion. Even in tumor regions with adequate oxygen supply, glycolysis and acid production are upregulated via the Warburg Effect [45], which results in an acidic extracellular pH (pHe) less than 6.0 in certain tumors (astrocytomas and squamous cell carcinomas) compared to normal tissue under physiologic conditions (pHe = 7.2-7.4) [44]. In our results, cap opening character is prominent at low pH values, which are especially for radiotherapies, as the latter will induce escalated pH value drop on cell death. Our confocal results also showed specific targeting and releasing of our dual-functionalized MSNs.

In summary, we reported a cancer-targeted nanosystem as biocompatible and effective sensitizer for radiosensitization, which may represent a significant step forward in the development of high-performance cancer theranostic upconversion nanoparticles. Utilization of new technologies has increased the radiation doses that can be safely administered for this purpose, which has resulted in improved control rates. Therefore, new approaches to sensitize CaP to radiotherapy are needed if clinical outcomes are to be further improved.

Acknowledgements

This work was supported by the National Natural Science Foundation of China (No. 81371470) and Shandong Provincial Natural Science Foundation of China (No. ZR2010HM080).

Appendix A. Supplementary Data

Supplementary data to this article can be found online at http://dx.doi.org/10.1016/j.tranon.2016.12.011.

References

[1] Barker CA, Bishop AJ, Chang M, Beal K, and Chan TA (2013). *Int J Radiat Oncol Biol Phys* **86**, 504–509.
[2] Omuro A and DeAngelis LM (2013). *JAMA* **310**, 1842–1850.
[3] Barani IJ and Larson DA (2015). *Cancer Treat Res* **163**, 49–73.
[4] Pan Y, Zhang Q, Atsaves V, Yang H, and Claret FX (2013). *Oncogene* **32**, 2756–2766.

[5] Huang Y, Luo Y, Zheng W, and Chen T (2014). *ACS Appl Mater Interfaces* **6**, 19217–19228.
[6] Marks PA and Xu WS (2009). *J Cell Biochem* **107**, 600–608.
[7] Hess-Stumpp H (2005). *Eur J Cell Biol* **84**, 109–121.
[8] Shabason JE, Tofilon PJ, and Camphausen K (2011). *J Cell Mol Med* **15**, 2735–2744.
[9] Van Nifterik KA, Van den Berg J, Slotman BJ, Lafleur MV, Sminia P, and Stalpers LJ (2012). *J Neuro-Oncol* **107**, 61–67.
[10] Gottlicher M, Minucci S, Zhu P, Kramer OH, Schimpf A, Giavara S, Sleeman JP, Lo Coco F, Nervi C, and Pelicci PG, et al (2001). *EMBO J* **20**, 6969–6978.
[11] Kostrouchova M, Kostrouch Z, and Kostrouchova M (2007). *Folia Biol* **53**, 37–49.
[12] Xu WS, Parmigiani RB, and Marks PA (2007). *Oncogene* **26**, 5541–5552.
[13] Chen X, Wong P, Radany E, and Wong JY (2009). *Cancer Biother Radiopharm* **24**, 689–699.
[14] Debeb BG, Xu W, Mok H, Li L, Robertson F, Ueno NT, Reuben J, Lucci A, Cristofanilli M, and Woodward WA (2010). *Int J Radiat Oncol Biol Phys* **76**, 889–895.
[15] Blattmann C, Oertel S, Ehemann V, Thiemann M, Huber PE, Bischof M, Witt O, Deubzer HE, Kulozik AE, and Debus J, et al (2010). *Int J Radiat Oncol Biol Phys* **78**, 237–245.
[16] Pourahmad J, Eskandari MR, Kaghazi A, Shaki F, Shahraki J, and Fard JK (2012). *Toxicol In Vitro* **26**, 545–551.
[17] Tong V, Teng XW, Chang TK, and Abbott FS (2005). *Toxicol Sci* **86**, 436–443.
[18] Auinger K, Muller V, Rudiger A, and Maggiorini M (2009). *Am J Emerg Med* **27** [1177 e1175–1176].
[19] Tung EW and Winn LM (2011). *Mol Pharmacol* **80**, 979–987.
[20] Chateauvieux S, Morceau F, Dicato M, and Diederich M (2010). *J Biomed Biotechnol* **2010**.
[21] Shahbazi MA, Herranz B, and Santos HA (2012). *Biomatter* **2**, 296–312.
[22] Mura S, Nicolas J, and Couvreur P (2013). *Nat Mater* **12**, 991–1003.
[23] Ganta S, Devalapally H, Shahiwala A, and Amiji M (2008). *J Control Release* **126**, 187–204.
[24] Shen Y, Tang H, Radosz M, Van Kirk E, and Murdoch WJ (2008). *Methods Mol Biol* **437**, 183–216.
[25] Tannock IF and Rotin D (1989). *Cancer Res* **49**, 4373–4384.
[26] Zhang H, Jiang Y, Zhao S, Jiang L, Meng Y, Liu P, Kim MO, and Li S (2015). *Med Chem Commun* **13**.
[27] Camphausen K, Cerna D, Scott T, Sproull M, Burgan WE, Cerra MA, Fine H, and Tofilon PJ (2005). *Int J Cancer* **114**, 380–386.
[28] Chinnaiyan P, Cerna D, Burgan WE, Beam K, Williams ES, Camphausen K, and Tofilon PJ (2008). *Clin Cancer Res* **14**, 5410–5415.
[29] Chu BF, Karpenko MJ, Liu Z, Aimiuwu J, Villalona-Calero MA, Chan KK, Grever MR, and Otterson GA (2013). *Blood* **71**, 115–121.
[30] Su JM, Li XN, Thompson P, Ou CN, Ingle AM, Russell H, Lau CC, Adamson PC, and Blaney SM (2011). *Clin Cancer Res* **17**, 589–597.
[31] Luo Z, Ding X, Hu Y, Wu S, Xiang Y, Zeng Y, Zhang B, Yan H, Zhang H, and Zhu L, et al (2013). *ACS Nano* **7**, 10271–10284.
[32] Kakuta T, Takashima Y, Nakahata M, Otsubo M, Yamaguchi H, and Harada A (2013). *Adv Mater* **25**, 2849–2853.
[33] Peng L, Peng X, Liu B, Wu C, Xie Y, and Yu G (2013). *Nano Lett* **13**, 2151–2157.
[34] Taratula O, Kuzmov A, Shah M, Garbuzenko OB, and Minko T (2013). *J Control Release* **171**, 349–357.
[35] Park S, Kang S, Chen X, Kim EJ, Kim J, Kim N, Kim J, and Jin MM (2013). *Biomaterials* **34**, 598–605.
[36] Zheng Q, Yang H, Wei J, Tong JL, and Shu YQ (2013). *Biomed Pharmacother* **67**, 569–575.
[37] Schroeder JE, Shweky I, Shmeeda H, Banin U, and Gabizon A (2007). *J Control Release* **124**, 28–34.
[38] Lee ES, Gao Z, Kim D, Park K, Kwon IC, and Bae YH (2008). *J Control Release* **129**, 228–236.
[39] Shi X, Thomas TP, Myc LA, Kotlyar A, and Baker Jr JR (2007). *Phys Chem Chem Phys* **9**, 5712–5720.
[40] Konner JA, Bell-McGuinn KM, Sabbatini P, Hensley ML, Tew WP, Pandit-Taskar N, Vander Els N, Phillips MD, Schweizer C, and Weil SC, et al (2010). *Clin Cancer Res* **16**, 5288–5295.
[41] Parker N, Turk MJ, Westrick E, Lewis JD, Low PS, and Leamon CP (2005). *Anal Biochem* **338**, 284–293.
[42] Naumann RW, Coleman RL, Burger RA, Sausville EA, Kutarska E, Ghamande SA, Gabrail NY, Depasquale SE, Nowara E, and Gilbert L, et al (2013). *J Clin Oncol Off J Am Soc Clin Oncol* **31**, 4400–4406.
[43] Jain RK (2002). *Semin Oncol* **29**, 3–9.
[44] Schornack PA and Gillies RJ (2003). *Neoplasia* **5**, 135–145.
[45] Estrella V, Chen T, Lloyd M, Wojtkowiak J, Cornnell HH, Ibrahim-Hashim A, Bailey K, Balagurunathan Y, Rothberg JM, and Sloane BF, et al (2013). *Cancer Res* **73**, 1524–1535.